Microstructural and mechanical study in the plastic zone of ARMCO iron processed by ECAP

Jairo Alberto Muñoz[a,*], Oscar Fabián Higuera[a,b], José María Cabrera[a]

[a] Department of Materials Science and Metallurgical Engineering, Universidad Politecnica de Catalunya, EEBE-c/Eduard Maristany 10-14, 08019 Barcelona, Spain
[b] Faculty of Engineering, Mechanical Engineering Program, Universidad del Atlántico, Barranquilla, Colombia

ARTICLE INFO

ABSTRACT

Plastic deformation of ARMCO iron processed by ECAP up to a maximum equivalent strain of sixteen (i.e., 1, 4, 8, and 16 ECAP passes) following route Bc was investigated by analyzing its microstructure and the stress-strain curves obtained after tensile tests at different levels of deformation. Three values of deformation (two in the plastic region taking into account the modified Crussard-Jaoul analysis and one after failure) were considered. Fractions of LAGB and HAGB, grain size and grain aspect ratio were calculated and compared for the different ECAP passes and tensile deformation levels. The dislocation density evolution calculated by the Bergström model for both the tensile curves and the ECAP curve showed a higher increase in the amount of dislocations during the initial stages of deformation than at higher values of deformation due to higher probabilities of dislocations annihilation. The strain hardening exponents calculated via the Bergström model for each ECAP pass shows that there is a continuous decrease in the strain hardening capacity until the eighth pass where a small increase with a subsequent stabilization was found. The dislocation densities calculated by the Estrin model presented a good correlation with values reported in bibliography for iron especially with those calculated by X-ray diffraction. This latter model predicted well the strain hardening evolution for stages III, IV and V for ARMCO iron processed by ECAP, where the main increments in hardening for stages IV and V were coming from the cell interiors.

1. Introduction

It is well known that dislocation cells can serve as subgrains precursors leading to nanocrystalline microstructures under severe plastic deformation. In particular, equal channel angular pressing (ECAP) is a promising severe plastic deformation (SPD) technique which allows the development of an ultrafine grain microstructure [1,2].

One of the mechanical characteristics of iron processed by ECAP is the lack of ductility. Since strain hardening is directly associated with formability, the study of the mechanisms responsible for strain hardening behavior is quite important. During large plastic deformation of metals and alloys, the original grain structure modifies its shape and size. Ultra fine grain (UFG) materials are quite attractive due to their attained ultrahigh strength, which is more than twice as that of their coarse grained counterparts. However, in general, UFG materials have an inherent mechanical drawback, i.e., a lack of strain hardening, resulting from the fact that the grain size is comparable to the dislocation cell size which corresponds to the dislocation mean free length [3]. In turn, this lack of hardening promotes a very limited

homogeneous ductility. Nevertheless, it has been established by Zehetbauer et al. [4] that for grain sizes higher than 20 nm the strength and strain hardening are still governed by dislocation mechanisms.

Most of the strain hardening models follows the concept pointed by Kocks [5] who derived macroscopic strain hardening from a constitutive description based on statistical generation, interaction and annihilation of dislocations. This type of model uses the total dislocation density as an internal variable provides an adequate description of stages II and III of strain hardening, but fails to cover stages IV and V that are predominant for large strains [6]. To study the strain hardening in stages IV and V the model proposed by Estrin et al. [7] which is based on the composite principle of Mughrabi et al. [8] has been instead used. In this model, Estrin et al. [9] did not distinguished between different types of dislocations but emphasized the dislocations exchange between cell interior and cell walls, and included a basic thermally activated contribution to stress. In contrast to the model of Zehetbauer [10], who postulated a constant volume fraction of cell walls, Estrin found that this volume fraction must decrease during stage IV in order to account for the nearly constant hardening coefficient characteristic of stage IV.

The aim of this work is the study of the mechanical and micro-

---

* Corresponding author.
E-mail addresses: jairomunoz8614@gmail.com (J.A. Muñoz), oscarhiguera@mail.uniatlantico.edu.co (O.F. Higuera), jose.maria.cabrera@upc.es (J.M. Cabrera).

structural properties of ARMCO iron, taken here as a BCC model material, processed through different number of ECAP passes following route Bc based on its strain hardening behavior through the above described different models and microstructural measurements in the plastic regime.

2. Experimental procedure

A commercial ARMCO iron (Fe-0.01%C-0.01%Si-0.059%Mn- < 0.01%P- < 0.010%S-0.02%Cr- < 0.005%Mo-0.038%Ni-0.013%Al (in wt%)) was received in the form of rods measuring 8 mm in diameter. The rods were divided into short billets having lengths of ~60 mm, which were subjected to severe plastic deformation by ECAP at room temperature. Previous to the deformation process, the samples were annealed at a temperature of 1203 K during 20 min in a tubular radiation heat furnace with a protective inert atmosphere of argon. ECAP was carried out using a solid die fabricated from tool steel with two channels intersecting at an inner angle of $\Phi = 90°$ and an outer angle of $\psi = 37°$, resulting in a strain of ~1 per pass according with the equation proposed by Iwahashi et al. [11].

The microstructure of the samples was characterized by Electron Backscattered Diffraction (EBSD). For this purpose, the specimens were cut from the centre of the ECAP samples and mechanically polished from 2500 grit SiC paper until 0.02 μm colloidal silica suspension, following standard metallographic procedures. Finally, to analyze the microstructural nature, the HKL CHANNEL 5 software was used to measure the grain size, the fraction of high and low angle grain boundaries (HAGB and LAGB respectively), and the aspect ratio. The misorientations lower than 0.5° were not considered in the data post-processing. The grains were defined using boundaries with misorientations, θ, larger than 15° and allowing completion down to 10°, and subgrains were defined by boundaries with misorientation larger than 2°.

Tensile tests at room temperature were performed using an universal testing machine equipped with a video camera extensometer. Three tensile specimens for each ECAP pass were tested at a constant crosshead velocity of $3.3*10^{-3}$ mm/s.

To detail the limited strain hardening, the microstructure was studied in different points of the stress – strain curve of samples previously ECAPed up to 0, 1, 4 and 16 passes. and tensile tested up to fracture. Then, once analysed the stress – strain curve, two additional samples were deformed under tensile conditions in the zone between the yield stress σ_Y and ultimate tensile stress σ_{UTS}. All three samples were mechanically analysed through the flow curves and microstructurally characterized by EBSD,

The mechanical analysis was performed by employing the modified Crussard-Jaoul analysis and the Bergström and Estrin models, which are briefly summarised in the following section.

2.1. Modified Crussard-Jaoul analysis

The modified Crussard-Jaoul analysis [12] is based on the classical Swift [13] Eq. (1).

$$\varepsilon = \varepsilon_0 + k_S \sigma^m \ or \ \sigma = \left(\frac{\varepsilon - \varepsilon_0}{k_s}\right)^{\frac{1}{m}} \tag{1}$$

where ε_0 is a material constant, k_S a strength coefficient and m a strain hardening exponent. The modified differential Crussard-Jaoul analysis takes the logarithmic form of Eq. (1), after differentiation with respect to ε, so that the strain hardening exponents can be obtained by a linear regression as follows:

$$ln(d\sigma/d\varepsilon) = (1-m)ln\sigma + ln(k_S m) \tag{2}$$

In the present work, it was observed that the work hardening rate according to this model was better explained by assuming two different

exponents at each testing conditions, as it can be confirmed in Fig. 6a and b of a previous study [14] where two slopes can be noticed in the plot ln $d\sigma/d\varepsilon$ vs the natural logarithm of stress or strain.

2.2. Bergström model

Since dislocations are the main responsible of the material's plasticity, the model proposed by Bergström [15] can give an approximation of the overall value of dislocation density ρ as a function of the strain, as show by Eq. (3):

$$\rho = \frac{U - A}{\Omega}(1 - e^{-\Omega\varepsilon}) + \rho_o e^{-\Omega\varepsilon} \tag{3}$$

where U is the composed rate at which mobile dislocations are immobilized or annihilated, A is the rate at which dislocations can be annihilated by reacting with other mobile and immobile dislocations as well as with grain boundaries, Ω expresses the probability of remobilization and annihilation through reactions between mobile and immobile dislocations and ρ_o is the dislocation density for $\varepsilon = 0$.

In this way, the relationship between the dislocation density and the flow stress is obtained by using the next equation:

$$\sigma = \sigma_{io} + \alpha Gb\sqrt{\rho} \tag{4}$$

Combining Eqs. (3) and (4) the final expression is:

$$\sigma = \sigma_{io} + \alpha Gb\left\{\frac{U - A}{\Omega}(1 - e^{-\Omega\varepsilon}) + \rho_o e^{-\Omega\varepsilon}\right\}^{\frac{1}{2}} \tag{5}$$

where σ_{io} is the friction stress, α is a constant with a value between 0.3 and 0.5, G is the shear modulus and b is the Burgers vector. Bergström also calculated the variation of the strain hardening exponent n with the deformation in the classical Hollom equation ($\sigma = \sigma_0 + K\varepsilon^n$) and obtained Eq. (6).

$$n = \frac{1}{2}\left(\frac{\varepsilon e^{-\Omega\varepsilon}}{1 + \frac{\sigma_{io}}{\sigma}}\right)\frac{U - A}{\rho}\left(1 - \frac{\rho_0}{\rho_{max}}\right) \tag{6}$$

where $\rho_{max} = U - A/\Omega$.

2.3. Estrin model

Another approach to determine the dislocation density evolution was proposed by Estrin et al. [9]. The essential difference of this model from the other models consists in a new rule predicting the evolution of the cell walls and the dislocations forming these walls. The following equations were proposed for the evolution of dislocations densities in cells ρ_c and dislocations within cell walls ρ_w:

$$\dot{\rho}_c = \alpha^* \frac{2}{3\sqrt{3}}\frac{\sqrt{\rho_w}}{b}\dot{\gamma}_w - \beta^* \frac{4\dot{\gamma}_c}{bd\sqrt{1 - f}} - k_o\left(\frac{\dot{\gamma}_c}{\dot{\gamma}_o}\right)^{\frac{-1}{n}}\dot{\gamma}_c\rho_c \tag{7}$$

$$\dot{\rho}_w = \frac{4\beta^*\dot{\gamma}_c\sqrt{1 - f}}{bdf} + \frac{2\beta^*\dot{\gamma}_c(1 - f)\sqrt{\rho_w}}{fb\sqrt{3}} - k_o\left(\frac{\dot{\gamma}_w}{\dot{\gamma}_o}\right)^{\frac{-1}{n}}\dot{\gamma}_w\rho_w \tag{8}$$

A new parameter here is the cell walls volume fraction f_w that varies with the change of the equivalent plastic strain which in turn follows an empiric law:

$$f_w = f_\infty + (f_0 - f_\infty)exp(-\gamma/\gamma^r) \tag{9}$$

The value of f can be calculated using the next equation developed by Estrin et al. [9]:

$$f_w = \frac{2wd - w^2}{d^2} \tag{10}$$

where w and d are the thickness and the cell size respectively.

Obviously not only the average dislocation density but also the flow stress over the volume unity should be calculated as:
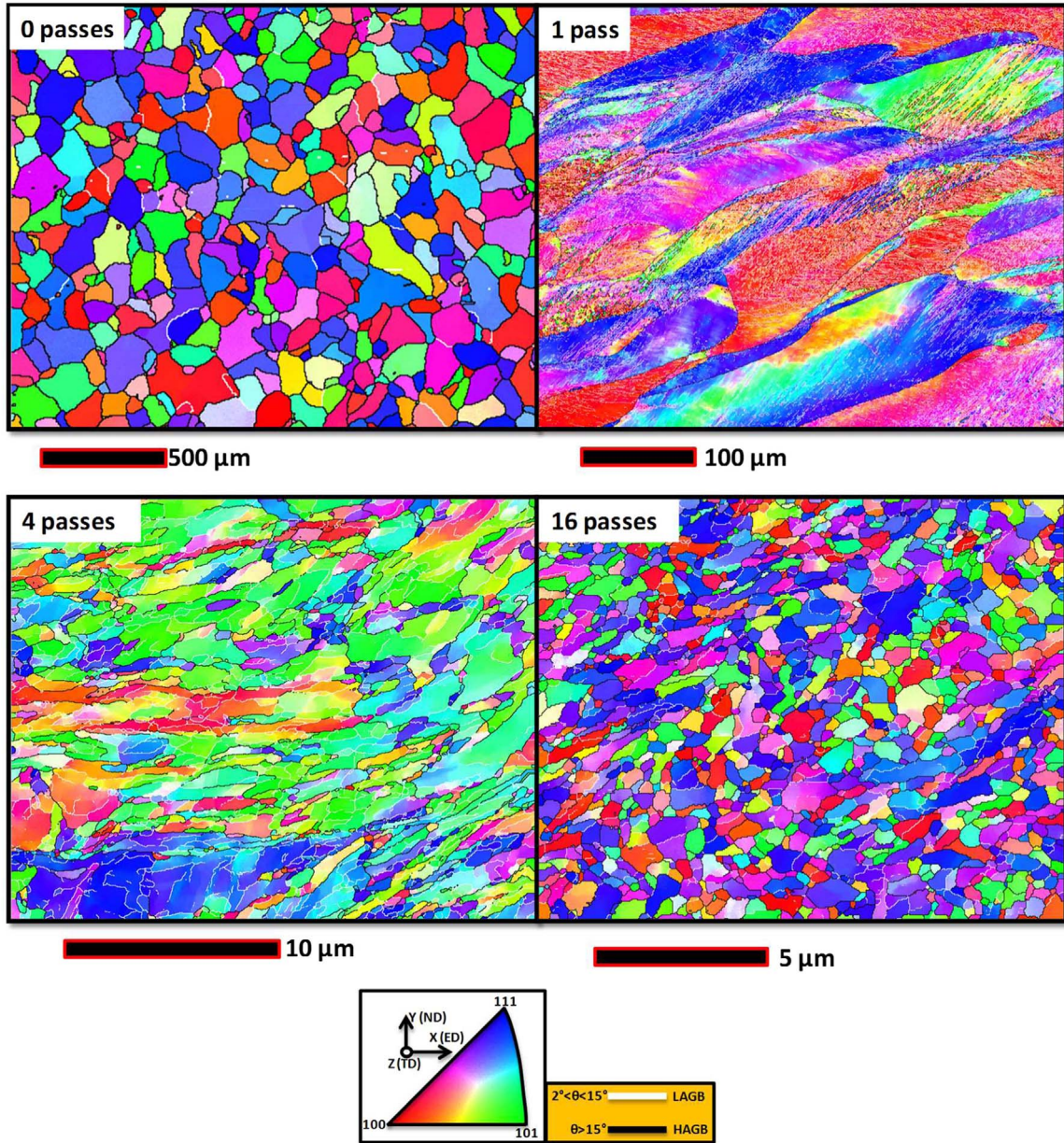
Fig. 1. Microstructures of the material after different ECAP passes.

$$\rho_{total} = f\rho_w + (1-f)\rho_c \tag{11}$$

$$\tau_t = f\tau_w + (1-f)\tau_c \tag{12}$$

The overall hardening rate can be identified as a result of three competing hardening components. Their individual contributions can be obtained by:

$$\theta^r = \frac{\partial \tau^r}{\partial \gamma^r} = \frac{\partial f}{\partial \gamma^r}(\tau_w^r - \tau_c^r) + f\frac{\partial \tau_w^r}{\partial \gamma^r} + (1-f)\frac{\partial \tau_c^r}{\partial \gamma^r}$$

$$\theta^r = \theta^f + \theta^w + \theta^c \tag{13}$$

where θ^f represents the softening caused by the volume fractions changes of the walls, while θ^w and θ^c accounts for the contributions to hardening produced in the walls and in the cell interiors, respectively.

3. Results and discussion

3.1. Microstructural properties

Fig. 1 shows the microstructural evolution for different ECAP passes. It can clearly be observed a reduction in the grain size from the initial condition to the final one (after sixteen passes). The initial annealed microstructure consists mainly of equiaxed grains and is basically formed by high angle grain boundaries (HAGB). The average grain size was ~72 µm. After one pass a sheared microstructure is observed together with a high fraction of LAGB. With further deformation (increasing the number of ECAP passes) most of the LAGB evolve into HAGB leading to an ultrafine-grain material. According to Tóth et al. [16] that evolution of LAGB into HAGB is a process of continuous dynamic recrystallization were new grain boundaries are created from geometrically necessary dislocations (GNDs).

One of the most important parameters of ultrafine materials is the grain size. Fig. 2a shows the evolution of the grain size as a function of the number of passes. It can be observed a large reduction from 72 µm in the annealed state to ~360 nm after sixteen ECAP passes. However, the biggest reduction is reached during the first passes (until the fifth pass), beyond this point a steady state is obtained. This saturation in the grain size evolution has been also found in different materials processed by severe plastic deformation [17–19]. This behavior can be explained
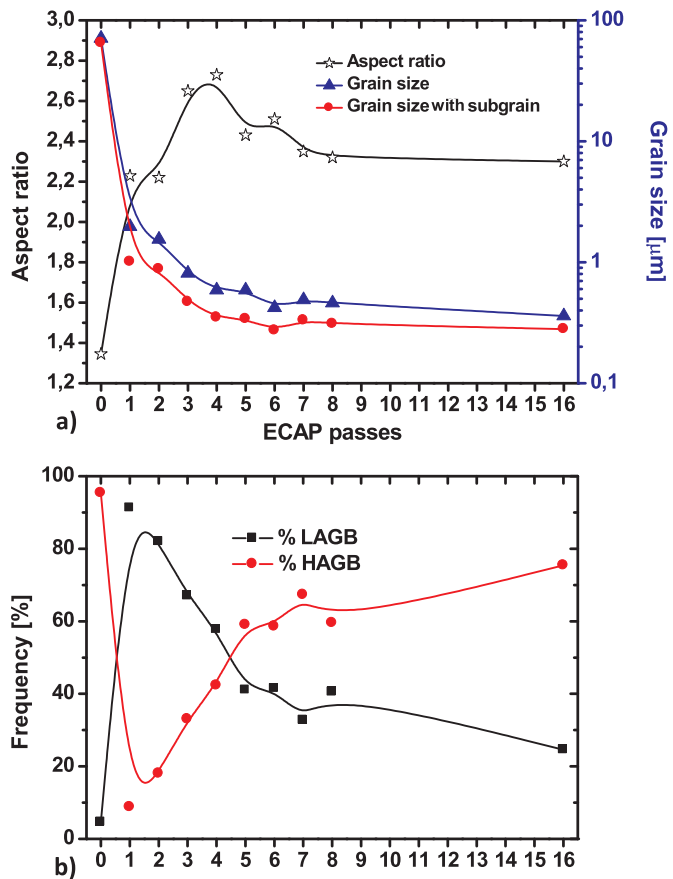
Fig. 2. Microstructure properties, a) grain size and aspect ratio, b) HAGB and LAGB fractions, for different number of passes by ECAP.
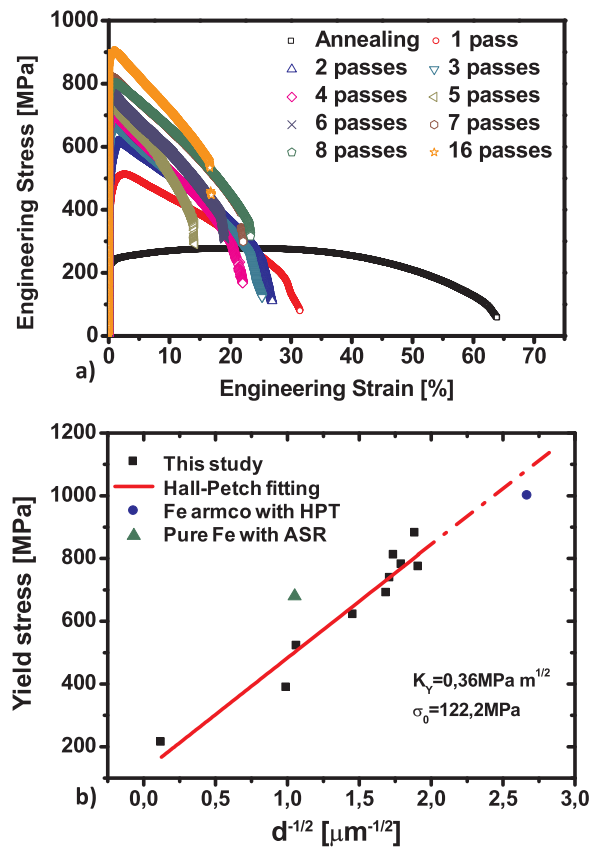

Fig. 3. a) Tensile flow curves after different ECAP passes, b) Hall-Petch fitting for the experimental data of the present ARMCO iron processed by ECAP. Green and blue points represent pure iron processed by asymmetric rolling (ASR) [25] and Armco iron processed by HPT [20] respectively. (For interpretation of the references to color in this figure legend, the reader is referred to the web version of this article).

by the balance reached between the generation of dislocations and the absorption of dislocations at grain boundaries. However, lower values of grain sizes (< 360 nm after sixteen passes) have been reported by other techniques of severe plastic deformation. Ivanisenko et al. [20] found a grain size of ~140 nm for ARMCO iron processed by high pressure torsion (HPT) while Valiev and Wetscher et al. [18,21] reported a grain size of about 80 nm after five revolutions of HPT at room temperature. One of the reasons for the difference in the grain size between ECAP and HPT of ARMCO iron is the hydrostatic pressure. According to Zehetbauer et al. [22] the hydrostatic pressure during the HPT process is higher than in the ECAP one, which leads to a greater reduction in the grain size. With respect to the grain aspect ratio, Fig. 2a shows an increase of the value until the fourth pass followed by a decrease until the eighth pass, where the aspect ratio levels out. The values of the aspect ratio for more than eight passes are quite similar to the values after one pass. This behavior indicates that the microstructure is not completely equiaxed even after sixteen passes. This is again in agreement with the fact that the ECAP process is not able to promote further reduction in the grain size even after sixteen passes. This lack of fully equiaxic microstructure allows to argue that, the microstructure has not reached its steady stage yet.

After the grain size evolution, a second important microstructure feature in ultrafine-grain materials is the misorientation distribution which in turns allow one to calculate the fraction of HAGB and LAGB (see Fig. 2b). In this latter figure two regimes can be seen, one dominated by the fraction of LAGB (less than five passes) and the second one dominated by the fraction of HAGB (more than five passes). This evolution of the HAGB fraction with the deformation is a consequence of the continuous transformation of LAGB because since in the initial stage of SPD processing, geometrically necessary boundaries are formed to subdivide the coarse grains into cell blocks [23]. For

that reason, in the first pass a high fraction of LAGB can be found, while in the following passes, HAGB number increases continuously (Fig. 2b).

3.2. Strength of the material

The effect of ECAP passes on the mechanical properties at room temperature, plotted in the form of stress-strain curves for different deformation levels is shown in Fig. 3a. In general, the ECAPed material showed the maximum strength at the early stage of deformation, followed by a region of plastic instability until failure. This softening is associated to the typical necking phenomenon which occurs during tensile tests. After four ECAP passes, a strong increase in strength with a significant decrease in ductility was observed. It is important to notice that the material with sixteen ECAP passes has ~3 times larger strength than the annealed material, reaching ~920 MPa which is quite similar to the values reported for a low carbon steel processed by ECAP by Park et al. [24]. In that investigation the authors determined a strength of ~900 MPa for a low carbon steel (Fe-0.15%C-0.25Si-1.1%Mn (in wt%)) processed up to 4 passes via route C at 500 °C. However, Ding et al. [25] reported a strength of 680 MPa in pure iron processed by asymmetric rolling (ASR). Those differences in strength with respect to the present material can be attributed to the fact that the low carbon steel presents a higher hardening capacity due to the mayor presence of alloying elements. On the other hand, the lower value of iron processed by ASR is a consequence of the lower and less homogeneous deformation introduced during each rolling with respect to the ECAP process.

It is well known that ultrafine-grain materials exhibit a large mechanical strength with respect to their coarse grain counterparts. This increase in strength is highly related to the grain refinement as already shown by the well-known Hall-Petch relation [26,27]:
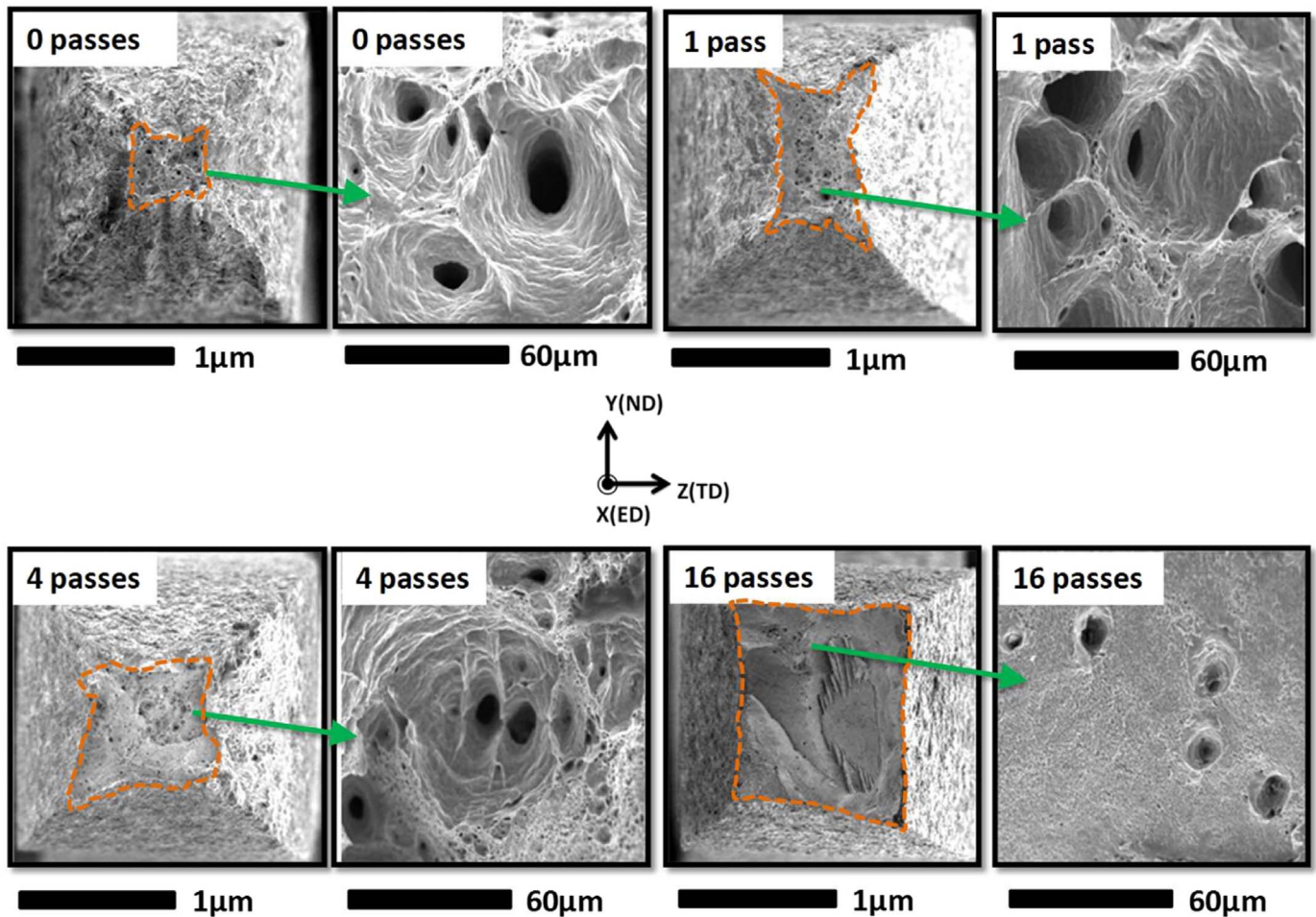
Fig. 4. Fracture surfaces after different ECAP passes.

$$\sigma_Y = \sigma_0 + \frac{K}{\sqrt{D}} \tag{14}$$

where D is the average grain size, σ_0 is the yield strength for very large grain size (single crystal) and K is a material constant. The Hall-Petch plot corresponding to the present experimental results is observed in Fig. 3b together with some other data of iron processed by ASR [25] and HPT [20]. The fitting of the data shows values of 0.36 MPa m$^{1/2}$ and 122.2 MPa for K and σ_0 respectively. Different values of K have been reported in the literature for iron. For example Anderson et al. [28] and Morrison et al. [29] established that the value of K for Armco iron and low carbon steels can vary between 0.55 MPa m$^{1/2}$ and 0.6 MPa m$^{1/2}$ respectively. However Valiev et al. [18] showed that for Armco iron under severe plastic deformation the best fitting was obtained with the value reported by Armstrong et al. [30] of 0.39 MPa m$^{1/2}$. The wide variation of this constant can be attributed to the purity grade of the iron, since it has been demonstrated by Takeda et al. [31] that only 60 ppm de carbon can change the value of K from 0.15 MPa m$^{1/2}$ to 0.6 MPa m$^{1/2}$.

Once can also noticed in Fig. 3b that the data reported by Ding and Ivanisenko [20,25] for iron are very close to the behavior obtained in this study. As already pointed out, the higher reduction in the grain size obtained in the Armco iron processed by HPT can be attributed to the higher hydrostatic pressure during this process which leads to a microstructure with a higher fraction of HAGB than by ECAP. On the other hand, the commercially pure iron processed by ASR [25] shows a higher strength than the Armco iron of this study for similar grain sizes. This strength difference can be attributed to the fraction of HAGB obtained by these two techniques, where a fraction of 60% in

comparison with 20% of HAGB was registered for the pure iron processed by ASR.

Several authors [32,33] have demonstrated that a major grain refinement, may lead to a very high hardness and strength in various metals and alloys, but nevertheless, these materials invariably exhibit low ductility under tensile testing. Additionally, it is important to note that SPD processing also leads to a lower reduction in the ductility than in more conventional deformation processing techniques such as rolling, drawing, and extrusion [34].

Typically, in the nanostructured metallic materials, plastic deformation localizes at the very earliest stages of strain ($< 3\%$), resulting in necking, followed by specimen failure. As illustrated in Fig. 4, the fracture surfaces on the current tensile specimens display a typical ductile appearance, ie. Voids and dimples coalescence, especially in specimens with 0, 1 and 4 ECAP passes. At increasing ECAP passes (i.e. 16 passes) fracture areas are characterized by surfaces with vein like patterns, which is characteristic of fracture via cleavage. However, dimples are still present. The presence of ductility features explains why although necking appears in the very early stages of deformation, the total elongation is still significantly large (close to 15%). For that reason, the lower homogeneous ductility observed in the present iron after ECAP can be related with lost in the strain hardening capacity as a consequence of the less efficiency in the dislocation motion and storage in the grain boundaries.

3.3. Plastic zone and strain hardening behavior

The lack of strain hardening of UFG materials is commonly explained by two factors: (a) the grain size is as fine as the dislocation
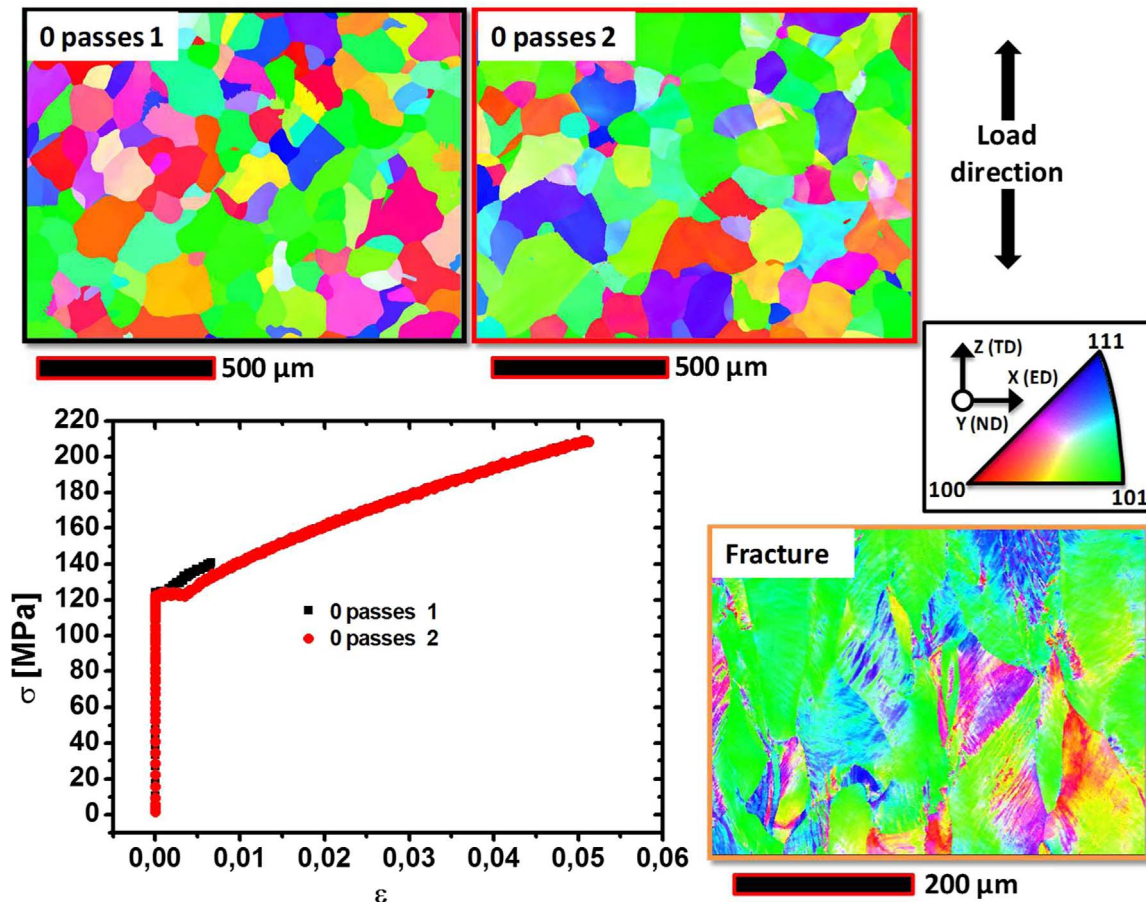
Fig. 5. Microstructures and tensile curves in the plastic zone for the initial material. In this case ECAP + TRACTION 1 correspond with 0 passes 1, ECAP + TRACTION 2 with 0 passes 2 and ECAP + FRACTURE with Fracture.

mean free path [35], and (b) under such condition, the dislocation generation rate is comparable to its annihilation rate, i.e. dynamic recovery compensates work hardening [36]. It has been pointed out that the efficient dislocation slip and dislocation storage within the grains can lead to a high strain hardening rate at low temperatures [37–40]. As estimated by Valiev et al. [40] the dislocation density in UFG could be increased by one order of magnitude in the early stage of deformation. This fact can be promoted especially when grain boundaries are in no equilibrium state [40,41].

3.3.1. Microstructure study in the plastic zone for UFG Armco iron

The microstructural and mechanical study of the plastic region for the current Armco iron at different levels of deformation was carried out from three selected points over the tensile curve (two in the zone of plastic homogeneous deformation and the third after the final fracture). The first two were chosen via the Modified Crussard-Jaoul analysis performed in a previous study [14]. As already mentioned, it was observed in this preliminary study that the strain hardening exponent of the modified Crussard-Jaoul model displayed two clear different values. Accordingly, one of the selected points of analysis corresponded to the region with the first slope, and the next selected point to the second slope. In other words, the values of deformation in the homogeneous plastic zone were defined as percentages lower and higher than the value of deformation were the slope change takes place (according with the modified Crussard-Jaoul model). The microstructures and tensile curves for the three points over the plastic zone for the materials with different number of ECAP passes are shown from Figs. 5–8.

The following notations were used: ECAP for the material deformed just with severe plastic deformation, ECAP + TRACTION 1 sample means materials that underwent SPD by ECAP (0, 1, 4 and 16 passes)

and then tensile tested up to point one (the first value of work hardening exponent). ECAP + TRACTION 2 means the same with the material tensile tested up to point 2 (i.e. after the change in the work hardening exponent according to the modified Crussard-Jaoul model). It should be mentioned that strain in TRACTION 2 is higher than in TRACTION 1 but lower that the deformation at the maximum stress. Additionally, the ECAP + FRACTURE TRACTION sample corresponds to the specimen tested up to failure.

In those figures (Figs. 5–8.) it can be mainly observed the change in the morphology and texture of the materials after the different deformation conditions, especially for the conditions ECAP + TRAC-TION 2 and ECAP + FRACTURE TRACTION, where microstructures with elongated grains in the tensile load direction were obtained. As well, in general, all the materials in the condition ECAP + FRACTURE TRACTION displayed a clear texture change in relation to the ECAP + TRACTION samples. This texture change shows that most of the grains after fracture are oriented towards the ⟨101⟩ direction with the exception of material with four ECAP passes, which showed a preferential orientation towards the ⟨111⟩ direction. The development of these preferential orientations is related with the presence of the γ (⟨111⟩∥ND) and α (⟨110⟩∥RD) fibers which are related to the recrystallization and cold deformation process of BCC materials [42].

In Fig. 9a the evolution of the grain size for each one of the conditions is indicated. It can be seen that the material in the ECAP + FRACTURE TRACTION condition shows a higher reduction in the grain size during the initial states (zero and one pass). However, for higher ECAP deformations (four and sixteen passes) the higher reduction in the grain size corresponds to the material in the condition ECAP + TRACTION 1. This behavior is in agreement with the obtained values of aspect ratio, where the highest and lowest values were observed in
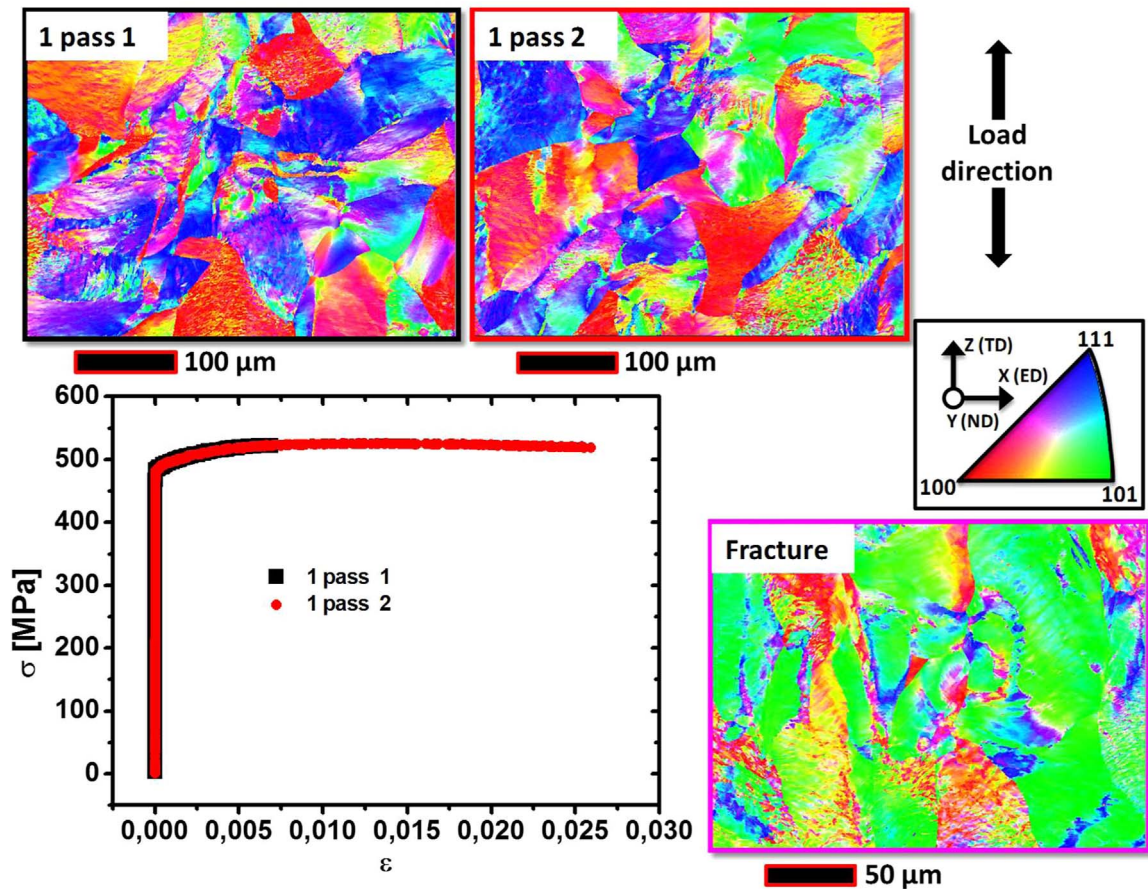
Fig. 6. Microstructures and tensile curves in the plastic zone for the material with one pass. In this case ECAP + TRACTION 1 correspond with 1 pass 1, ECAP + TRACTION 2 with 1 pass 2 and ECAP + FRACTURE with Fracture.

the condition of ECAP + FRACTURE TRACTION and ECAP + TRACTION 1 respectively, as shown in Fig. 9b.

The evolution of the grain size (Fig. 9a) also reveals that during the tensile test, the materials with less than 2 ECAP passes do not present a significant change in the grain size in the plastic zone, whereas, an evident grain size change in the plastic zone is noticed for materials with more than three ECAP passes. This observation could indicate the occurrence of dynamic recovery in the samples with more than 3 ECAP passes, which could be the main responsible mechanism of the reduction of the strain hardening capacity. This behavior is coherent with the values of strain hardening exponents calculated in a previous study [14], where higher values in the initial state of tensile flow curve were obtained for the specimens after ECAP processing according with the modified Crussard-Jaoul analysis. When representing the grain sizes obtained for each conditions (Initial stage, ECAP, ECAP + TRACTION 1, ECAP + TRACTION 2 and ECAP + TRACTION FRACTURE) in a Hall-Petch plot, Fig. 10a, it can be observed that in the ECAP + TRACTION 1 condition a larger reduction in the grain size occurs rather than in the other conditions for the materials with more than 4 passes. This confirms that there is a higher material hardening during the initial stages of deformation than during the final stages (i.e. ECAP TRACTION 2).

Another consequence of the additional deformation through the tensile test is the increment in the fraction of HAGB for the ECAP + TRACTION 1 and ECAP + TRACTION FRACTURE conditions, as shown in Fig. 10b. The increment for the latter case can be attributed to the total plastic deformation until failure, that is, at less 15% of engineering strain as confirmed by Fig. 3a. On the other hand, the increment of HAGB fraction in the ECAP + TRACTION 1 condition is coherent with the reduction in the grain size which also produces the

increment in the strain hardening in the first stage of plastic deformation. This behavior is coherent with the model developed by Hughes et al. [43] where the Hall-Petch relationship was evaluated taking into account the influence of the two types of boundaries, high angle boundaries between grains and low angle grain boundaries. It has been reported in another study by Rodriguez et al. [19] that the most important strength contribution for UFG copper processed at room temperature is coming from LAGBs.

According to Hughes et al. [43] the evolution of dislocation stored in LAGBs can be calculated with the next equation:

$$\rho_{LAGB} = \frac{3(1-f)\overline{\theta}_{LAGB}}{bL} \tag{15}$$

where f is the HAGB fraction, $\overline{\theta}_{LAGB}$ the average misorientation of the LAGB and L the average boundary spacing of subgrains. All these parameters can be easily calculated from the EBSD measurements. Accordingly, the dislocation densities calculated for each one of the conditions established by the modified Crussard-Jaoul analysis are shown in Fig. 11. The values calculated for the material in the ECAP condition are higher than for the rest of the conditions. However, all the conditions present an increasing behavior until the fourth pass followed by a continuous decrease until the sixteenth pass.

Two important aspects can be highlighted. The first is the fact that the dislocation densities in the material after tensile tests are smaller than after ECAP, which could be attributed to the generation of new grain boundaries from the dislocations stored in the LAGBs as a consequence of the additional plastic deformation introduced during the tensile test. The second important factor is that there is an evident reduction in the dislocations stored in LAGBs, due to the continuous increase in the HAGB fraction with the increase in the deformation. It is
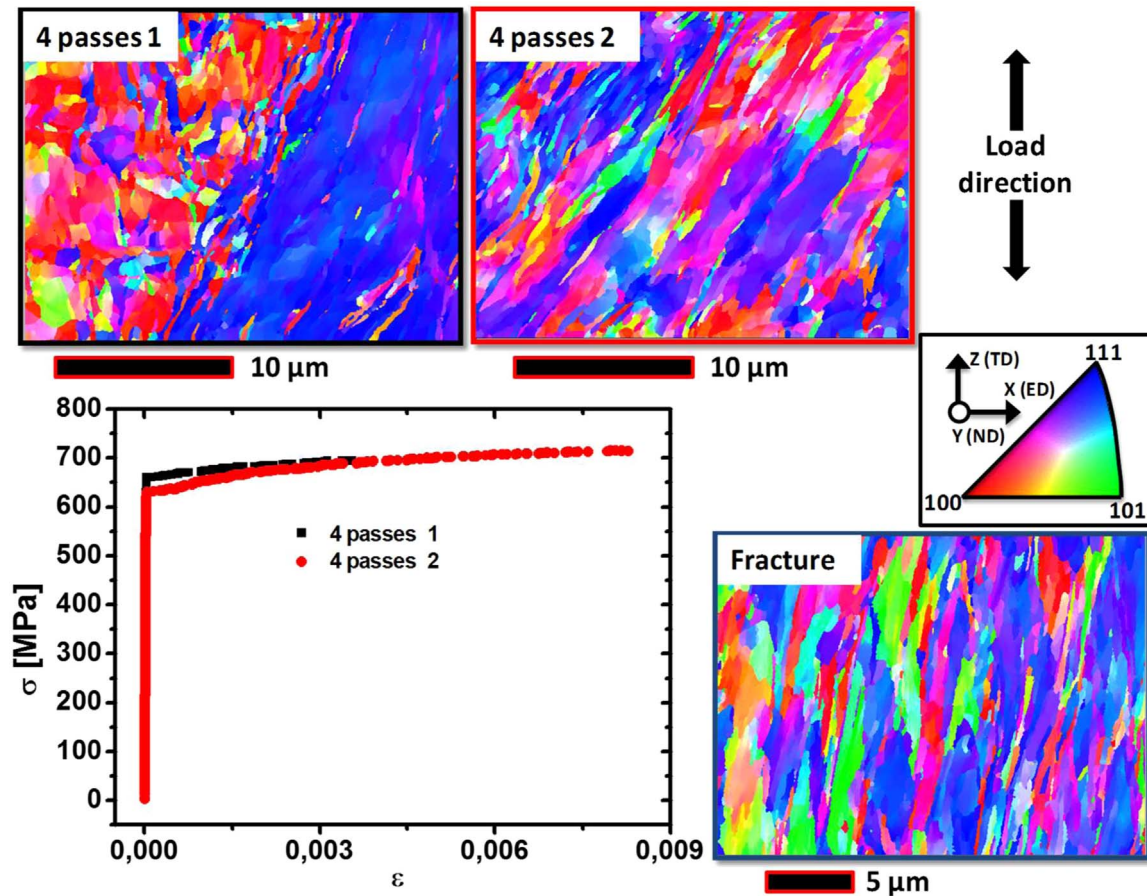
Fig. 7. Microstructures and tensile curves in the plastic zone for the material with four passes. In this case ECAP + TRACTION 1 correspond with 4 passes 1, ECAP + TRACTION 2 with 4 passes 2 and ECAP + FRACTURE with Fracture.

important to notice that the reduction in the dislocations in the first stage of the tensile tests (ECAP + TRACTION 1) is smaller than in the second stage (ECAP + TRACTION 2). This shows that during the tensile test the strength contributions are most important during the initial stages of deformation than from the second stage.

3.3.2. Bergström model

To better understand the plastic behavior, an analysis using the dislocation density was performed. Using Eq. (5) the evolution of the dislocation density for the tensile samples and for the simply ECAPed materials can be obtained. In Eq. (5), α is a constant which can take values between 0.3 and 0.5 [44], ρ_0 is the dislocation density between borders, that can take a value of $\rho_0 = 10^{12} \, \text{m}^{-2}$ for an annealed material [45]. The value of σ_{io} was obtained using the yield stress for the annealed material (without any deformation) through the Eq. (5).

The calculated dislocation density values are summarized in Fig. 12a, and in Fig. 12b the variation of the constant Ω for the ECAP and the tensile samples is shown. Both conditions (just ECAP, and ECAP + tensile test), are compatible with growing dislocation density with the deformation. It can be seen in Fig. 12a that for the materials with five and six passes followed by tensile tests, the dislocation densities are relatively constant, which is coherent with the tensile curves where the homogeneous plastic zone in these two materials is absent. According to the Bergström model the constant Ω can be related with the probability of remobilization and annihilation of dislocations through reactions with themselves and with the grain boundaries. From Fig. 12b it can be determined that the higher values of this constant are obtained for the materials with five and six passes followed by tensile test, which would explain the dislocations reduction with increased deformation. For that reason, those values would indicate a higher annihilation rate

of dislocations which in turns could be attributed to the existence of a heterogeneous microstructure of LAGB and HAGB where there is not a clear dominant fraction (see Fig. 2b). However, for the simply ECAPed specimen a value just higher than the value obtained for the annealed material after the tensile test is observed in Fig. 12b. This means that the material could still present more interaction of dislocations either with themselves or with the grain boundaries after sixteen passes leading to further grain size reduction at larger strain. In other words, it means that our material could stand more deformation from other process of SPD leading to a more stable microstructure.

The strain hardening behavior for the material with different passes as well as after tensile test is also indicated in Fig. 13 (ECAP curve, the yield stress for different number of passes and the curve for each pass after tensile deformation) via Eq. (6). As estimated by Valiev et al. [40] the dislocation density in UFG materials could be increased from 10^{14} to $10^{15} \, \text{m}^{-2}$ in the early stage of deformation. This can explain the initial deformation stage with high strain hardening rate (Fig. 13, ECAP curve). This deformation process can be promoted especially when GBs are in non-equilibrium state [40,41]. For that reason, the materials after 1, 2 and 3 passes show the highest strain hardening (Fig. 13) due to the presence of high fractions of LAGB as displayed in Fig. 2b. The strain hardening curves for the samples processed solely by ECAP show the maximum values in the beginning of the deformation followed by a continuous decreasing behavior. This is quite similar to the behavior predicted by the modified Crussard-Jaoul analysis where the strain hardening exponents in the initial stage of deformation were higher than in the second one. As it is seen in Fig. 13 the main hardening of the ECAP curve is produced until the first ECAP pass where also the highest increase in the dislocation density is obtained. Whereas, after the first pass in the ECAP curve a continuous decrease in the hardening
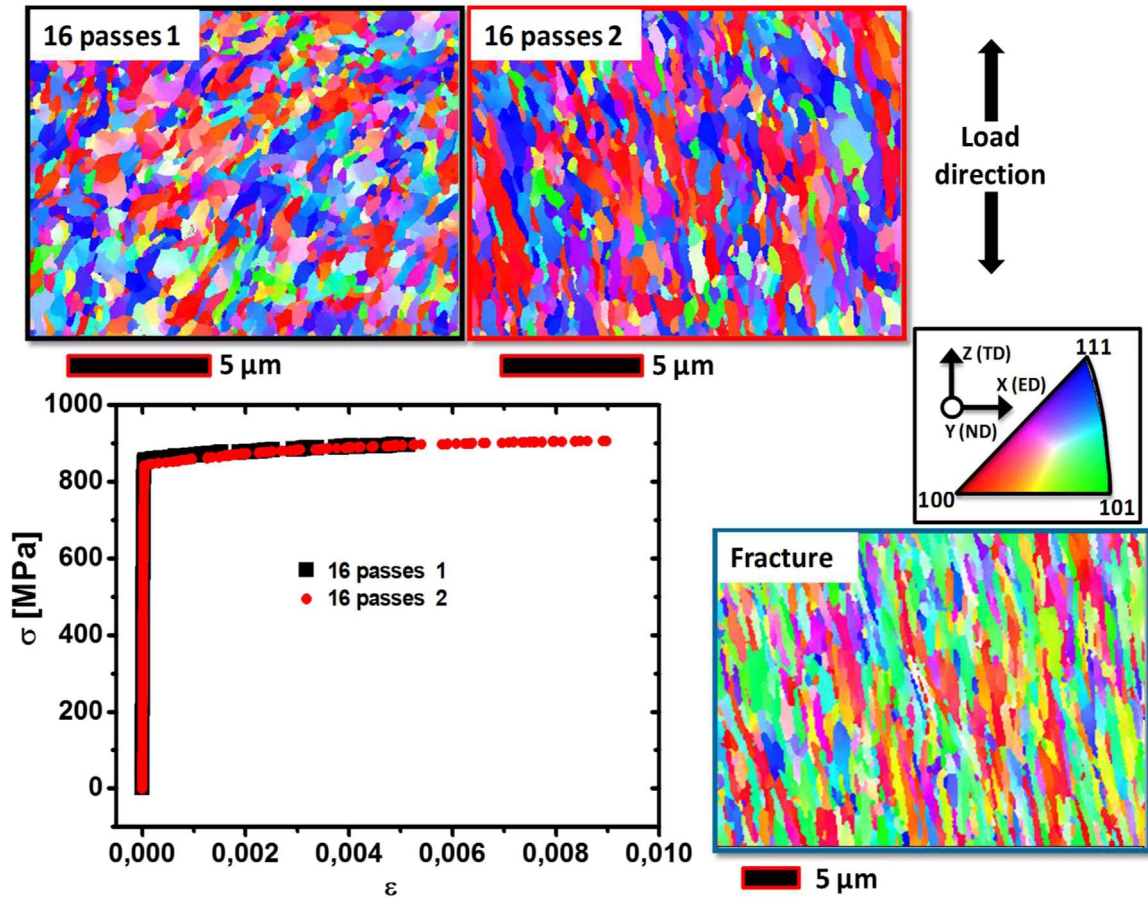
Fig. 8. Microstructures and tensile curves in the plastic zone for the material with sixteen passes. In this case ECAP + TRACTION 1 correspond with 16 passes 1, ECAP + TRACTION 2 with 16 passes 2 and ECAP + FRACTURE with Fracture.

exponent until the sixteenth pass can be seen. This behavior is similar for the strain hardening exponent during the tensile test. However, it should be mentioned that most of the values of the strain hardening exponents for the traction test until the third pass are higher than those for the annealed material. The decreasing behavior in the strain hardening exponents for the material with ECAP and traction can be attributed, according with the Bergström model, to the increase in the constant Ω which could be related to the annihilation rather than the remobilization of dislocation. But the fact that the values of the strain hardening exponent are smaller for the annealed iron than during the first three passes is a consequence of the increase in the dislocation densities stored in LAGBs.

3.3.3. Estrin model

The original model proposed by Estrin et al. [9] and modified by Tóth et al. [46] has been used to know more about the mechanical response of ultrafine grain iron. According to this model the total dislocation densities can be calculated as the sum of the dislocations inside of the cells and the dislocations inside of the cell walls. The evolution of the volume fraction of cell walls for the present results is shown in Fig. 14. The values were obtained using Eq. (10) through EBSD measurements. Fig. 14 shows that f_w uniformly decreases with strain, asymptotically tending to saturation at large strains as Müller et al. [47] and Zehetbauer and Ungar [48] predicted.

The evolution of dislocation density is obtained solving Eqs. (7) and (8). The values and descriptions of the variables used in this model are shown in Table 1. The values obtained for the dislocation density as a function of deformation can be seen in Fig. 15a together with other

values reported in literature for iron calculated by transmission electron microscopy after ECAP [49] and via X-ray diffraction after cold working [50] as well as the previous values calculated with the Bergström model. The dislocation densities in the cell walls and cell interiors rose to over 10^{16} and $10^{15}\,\text{m}^{-2}$, respectively. Correspondingly, the total dislocation densities increased to $2.45 \ast 10^{15}\,\text{m}^{-2}$ after sixteen ECAP passes as noticed from Fig. 15a.

The comparisons of the values obtained via the Estrin model with other values for iron obtained by TEM, XRD and with the Bergström model show that the values calculated with the Bergström model are quite similar to the values in the cell walls calculated with the Estrin model. This could be attributed to the fact that the Bergström model has a basic approach in the evolution of the flow stress and it does not take into account other factors like the mechanism of dynamic recovery and also the fraction of operative Frank Read sources due to dislocations coming from the walls (α^*). Perhaps one the most important parameters is the variation of the volume fraction of cell walls with deformation which has an important role especially at high deformations (stage IV). On the other hand the values calculated via XRD by Schafler et al. [50] are in good agreement with the current values of total dislocations calculated via the Estrin model. However, the values calculated with TEM by Ivanov et al. [49] are different with respect to the values calculated in this investigation. This can be attributed, to the difficulty to quantify the densities in the walls by TEM therefore leading to lower values of the dislocation densities. It can also be observed in Fig. 15b the good correlation between the experimental and calculated values (based on Eq. (12)) of the yield stress for different values of deformation.
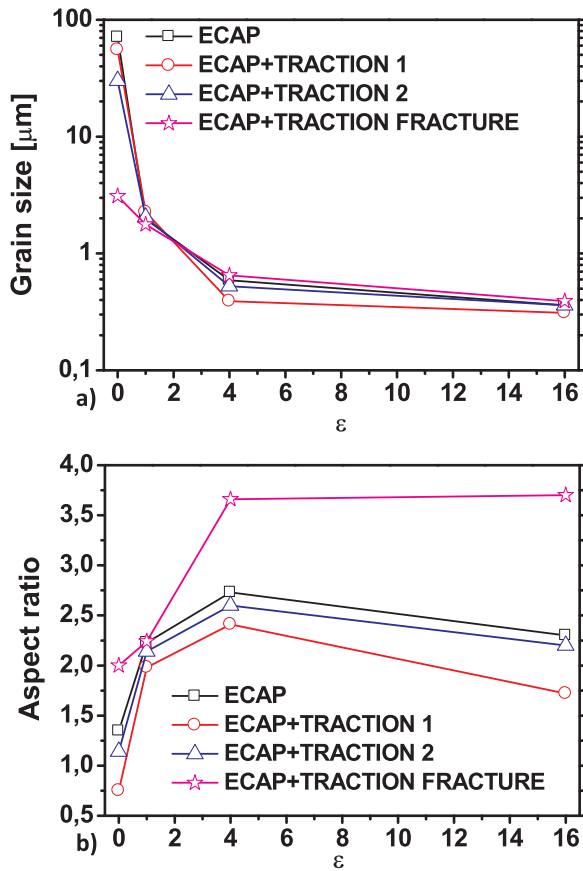
Fig. 9. Microstructural properties, a) grain size and b) aspect ratio evolutions as a function of the ECAP passes after different testing conditions.
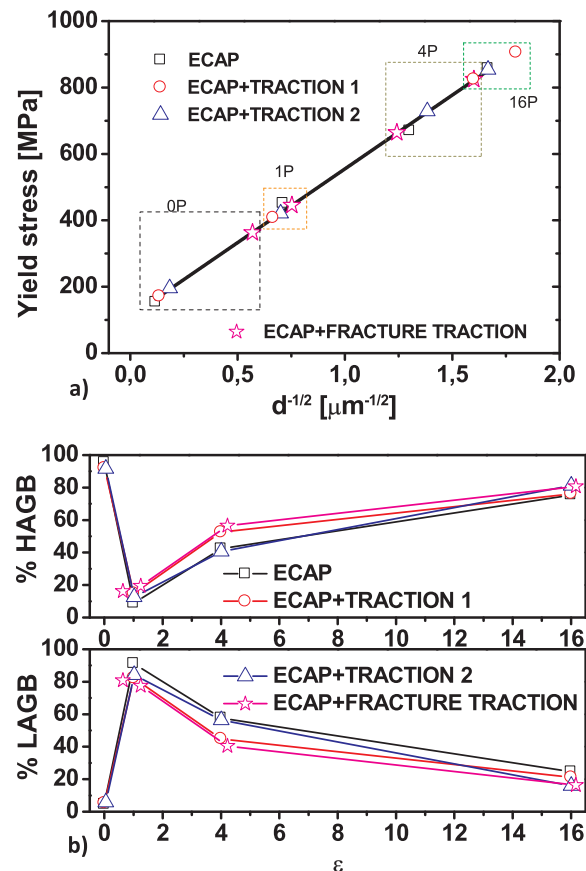

Fig. 10. a) Hall-Petch plot and b) HAGB and LAGB fractions for the materials after traction.

Finally, Fig. 16 presents the strain hardening rate curve together with the different hardening contributions according to the Estrin model. During the initial stages of deformation, a continuous decrease in the strain hardening rate corresponding with the stage III is observed (Fig. 16a), where the contributions of hardening coming from the walls and interiors of cells are in the same proportions (as seen in Fig. 16b) whereas, the softening contribution is not really important in this stage. The stage IV is characterized by a nearly constant hardening rate as it seen in Fig. 16a, where the softening component, generated by the decrease in the volume fraction of cell walls, becomes more important (Fig. 16b) with its pronounced reduction at the beginning of the stage IV. On the other hand, the proportion of cell wall hardening exhibits a maximum at the beginning of the stage IV followed by a continuous and significant decrease. In contrast, the hardening contribution of the cell interiors increases continuously, similar with the results of Argon et al. [51] and Tóth et al. for copper [46].

The occurrences of stage IV correspond with the material deformation after two passes, which is in good agreement with results of the other models presented before. This behavior also showed that the material hardening was more important during the first ECAP passes. However, in the previous models (modified Crussard-Jaoul and Bergström) was found an increase in the hardening capacity of the material after eight passes. This was also found in Estrin's model, where a similar behavior in the strain hardening contributions at the beginning of the stage IV was observed in the stage V. For that reason in Fig. 16a, a small plateau similar to the one in stage IV can be observed. This behavior is reflected in the strain hardening contributions especially in the reduction of the softening contribution (i.e. higher values of θ^f/θ^r).
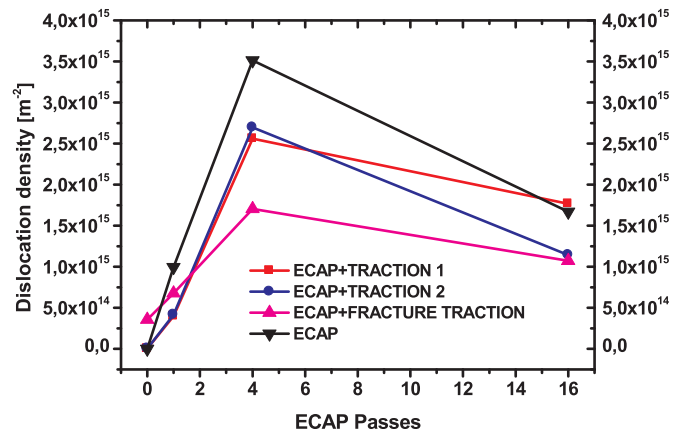

Fig. 11. Dislocation density stored in LAGBs.

4. Conclusions

A quite considerable reduction in the grain size from the initial condition (72 μm) to the final after sixteen passes (~360 nm) was obtained for the ARMCO iron processed by ECAP. The biggest reduction was reached during the first five passes. Beyond this point a steady stage was apparently obtained. This behavior was explained by the balance reached between the generation of dislocations and the absorption of dislocations at grain boundaries. In this way, the flow stress also presented the main increments during the first passes. In
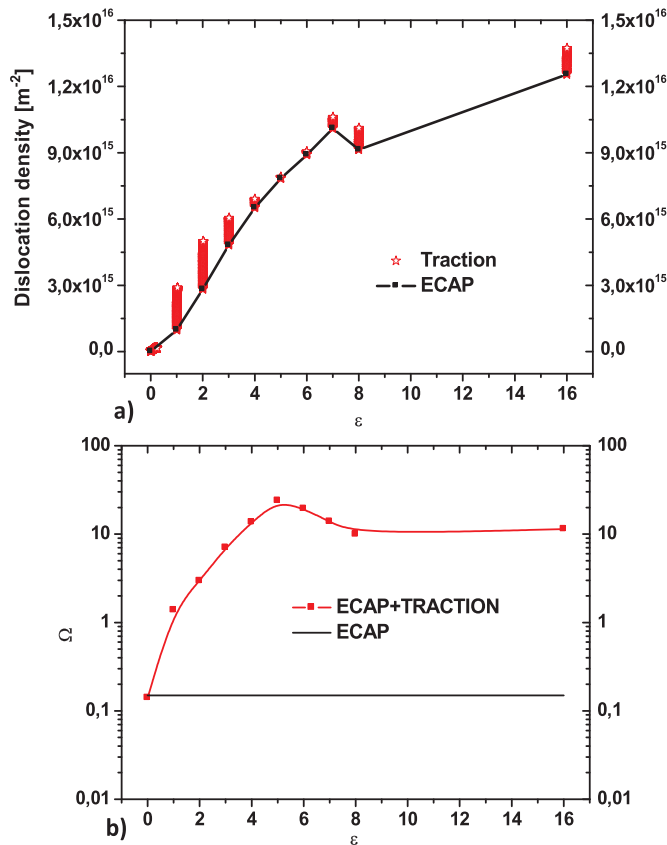
Fig. 12. Bergström model, a) dislocation densities for the ECAP and tensile curves, b) variation of the Ω constant.
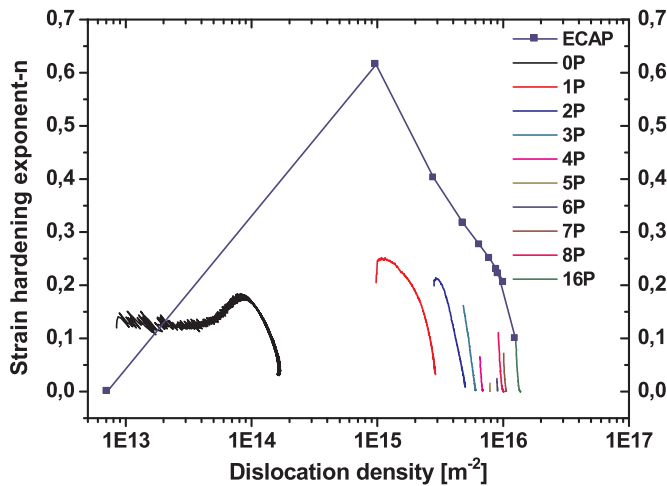

Fig. 13. Strain hardening exponent evolution for the ECAP and tensile curves.

Fig. 14. Volume fraction of cell walls.

Table 1
Parameters of the Estrin model.

Parameter	Value	Brief explanation
b	$2,48*10^{-10}$ m	Magnitude of Burgers vector for Fe
G	82,000 MPa	Shear modulus Fe
f_0	0.34836	Initial value for f
f_∞	0.08986	Final value for f
K	> 0	Proportionality between d and $1/\sqrt{\rho_T}$
α	0.3	Constant between 0,3 and 0,5
$\dot{\gamma}$	> 0	Plastic shear strain rate
$\dot{\gamma}_0$	> 0	Reference shear strain rate
α^*	0.06	Fraction of active Frank-Read sources
β^*	0.012	Emigrating fraction of ρ_C
$\rho_w^{(t=0)}$	10^{14} m^{-2}	Initial value for dislocations in the walls
$\rho_c^{(t=0)}$	$5*10^{13}$ m^{-2}	Initial value for dislocations inside of cells
n	> 0	Dynamic recovery exponent

general, the ECAPed materials showed the maximum strength at the early stage of deformation, followed by a region of plastic instability until failure. Material with sixteen ECAP passes presented an increment of ~3 times in strength with respect to the annealed material, but, and elongation until the maximum stress lower than 2%.

The lack of ductility with the increase in the deformation by the ECAP process was attributed to the lost of the strain hardening capacity, being the reduction in the grain size the main responsible, and in turns
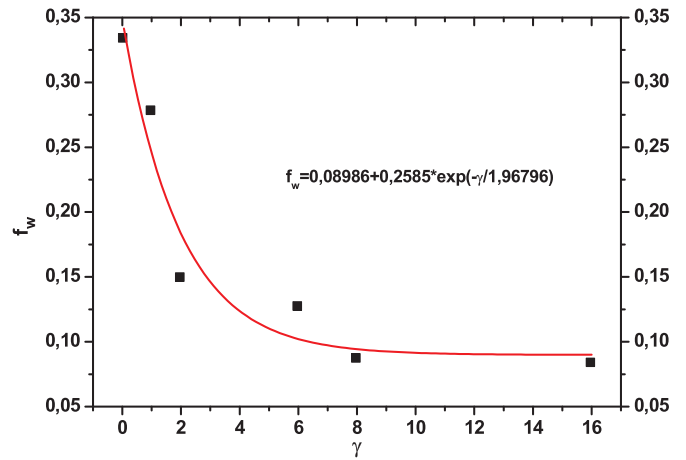
causing the occurrence of dynamic recovery due to the great increment in the dislocation density during the first passes leading to less efficiency in the dislocation motion and storage for higher deformations (more than four passes).

The study in the plastic zone after tensile test showed changes in the grain size and in the material texture. The grain size evolution was found to be higher in the initial stages of the tensile test (ECAP +TRACTION 1 condition) for the materials with zero and one pass. However, for the materials with more than four passes the opposite happens indicating that dynamic recovery takes more importance. On the other hand, it was found a texture change with respect to the materials before tensile test, specially for the microstructures until rupture, where most of the grains were oriented towards ⟨101⟩ or ⟨111⟩ direction indicating the presence of continuous recrystallization.

The Bergström model showed a continuous increment in the dislocation density with the number of ECAP passes, where the higher increments were obtained during the first passes (0–5 passes). On the other hand, the application of the Bergström model over the tensile curves for different number of ECAP passes showed and increment in the dislocation densities with the increment in the deformation where the materials with five and six passes presented the lowest increments. This behavior was coherent with the higher values of Ω and the reduction in the strain hardening exponent obtained for those materials, indicating the higher possibility of dislocation annihilation instead
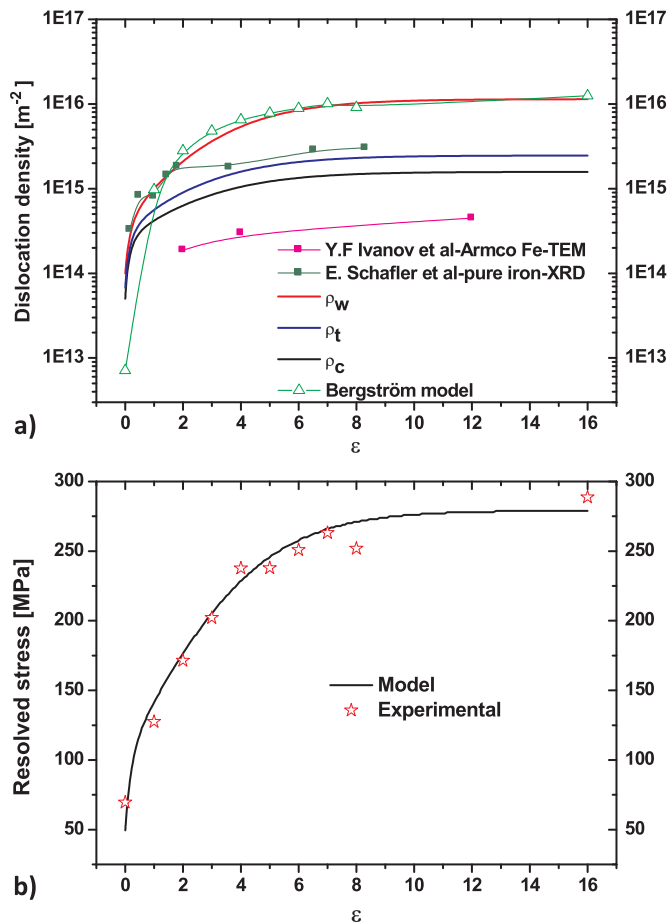
Fig. 15. Estrin model, a) dislocation densities evolution for iron together with other values reported in literature for iron calculated by TEM [49], X-ray diffraction [50] and via the Bergström model and b) experimental and model values obtained for the ECAP curve.

Fig. 16. a) Strain hardening rate and b) relative hardening contributions of the cell walls θ^w/θ^r, cell interiors θ^c/θ^r as well as the softening caused by the decrease of the volume fraction of the cell walls θ^f/θ^r.

of multiplication. The Ω coefficient obtained for the ECAP curve showed a quite similar value to the material with zero passes after traction and the strain hardening exponent evolution showed an increasing behavior until the first pass followed by a continuous decrease.

Estrin model showed that the evolution of the strain hardening at high deformations (stage IV) depends of the cell walls volume fraction evolution. In this way, the strain hardening contributions from the walls and interiors together with the softening contribution from the cell walls volume fraction indicated that during the stage III the contributions of hardening coming from the walls and interiors of cells were in the same proportions whereas, the softening contribution was not really important in this stage. On the other hand, the stage IV was characterized by a nearly constant hardening rate where the softening component, generated by the decrease in the volume fraction of cell walls, became more important with its pronounced reduction at the beginning of the stage IV. On the other hand, the cell wall part of hardening exhibited a maximum at the beginning of the stage IV followed by a continuous and significant decrease. In contrast, the hardening contribution of the cell interiors increased continuously. This model also showed the occurrence of stage V with the appearance of a small plateau at the end of the stage IV.

Acknowledgements

References

[1] V.M. Segal, Materials processing by simple shear, Mater. Sci. Eng. A 197 (1995) 157.
[2] L.S. Tóth, Y. Estrin, R. Lapovok, C. Gu, Acta Mater. 58 (5) (2010) 1782–1794.
[3] Y.I. Son, Y.K. Lee, K.-T. Park, C.S. Lee, D.H. Shin, Acta Mater. 53 (2005) 3125–3134.
[4] M.J. Zehetbauer, Y. Estrin, Modeling of strength and strain hardening of bulk nanostructured materials, in: M.J. Zehetbauer, Y.T. Zhu (Eds.), Bulk Nanostructured Materials, WILEY-VCH Verlag GmbH & Co. KGaA, Weinheim, 2009, p. 109.
[5] U.F. Kocks, J. Eng. Mater. Technol. 98 (1976) 76.
[6] M. Zehetbauer, Y.V. Seumer, Acta Metall. Mater. 41 (1993) 577.
[7] Y. Estrin, L.S. Toth, A. Molinari, Y. Brechet, Acta Mater. 46 (1998) 5509–5522.
[8] H. Mughrabi, Acta Metall. 31 (1983) 1367.
[9] Y. Estrin, L. Tóth, A. Molinari, Y. Bréchet, A dislocation-based model for all hardening stages in large strain deformation, Acta Mater. 46 (1998) 5509–5522.
[10] M. Zehetbauer, Acta Metall. Mater. 41 (1993) 589.
[11] Y. Iwahashi, Z. Horita, M. Nemoto, T. Langdon, Acta Mater. 46 (1998) 3317.
[12] R.E. Reed-Hill, W.R. Cribb, S.N. Monteiro, Metall. Trans. 4 (1973) 2665–2667.
[13] H.W. Swift, Plastic instability under plane stress, J. Mech. Phys. Solids 1 (1952) 1–18.
[14] J. Muñoz Bolaños, O. Higuera Cobos, J. Cabrera Marrero, Strain hardening behavior of ARMCO iron processed by ECAP, IOP Conf. Ser.: Mater. Sci. Eng. 63 (2014) 012143.
[15] Y. Bergstrom, A dislocation model for stress-strain behavior of polycrystalline alfa-Fe with special emphasis on the variation of the densities of mobile and immobile dislocations, Mater. Sci. Eng. 5 (1969/70) 193–202.
[16] L.S. Toth, C. Gu, Ultrafine-grain metals by severe plastic deformation, Mater. Charact. 92 (2014) 1–14.
[17] O.F. Higuera-Cobos, J.M. Cabrera, Mater. Sci. Eng. A 571 (2013) 103–114.
[18] R.Z. Valiev, Y.V. Ivanisenko, E.F. Rauch, B. Baudlet, Acta Mater. 44 (1996) 4705.
[19] P. Rodríguez-Calvillo, N. Ferrerc, J.M. Cabrera, J. Alloy. Compd. 626 (2015) 340–348.
[20] Y. Ivanisenko, A.V. Sergueeva, A. Minkow, R.Z. Valiev, H.-J. Fecht, Mechanical properties and thermal stability of nano-structured ARMCO iron produced by high pressure torsion, in: M. Zehetbauer, R.Z. Valiev (Eds.), Nanomaterials by Severe

Plastic Deformation, Wiley-VCH Verlag GmbH & Co. KGaA, Weinheim, 2004.
[21] F. Wetscher, R. Pippan, Philos. Mag. 86 (2006) 5867.
[22] M. Zehetbauer, H. Stüwe, A. Vorhauer, E. Schafler, J. Kohout, The role of hydrostatic pressure in severe plastic eformation, Adv. Eng. Mater. 5 (5) (2003).
[23] Y. Tomita, K. Okabayashi, Metall. Trans. A16 (1985) 865.
[24] K.-T. Park, S. Han, B. Ahn, D. Shin, Y. Lee, K. Um, Scr. Mater. 51 (2004) 909–913.
[25] Y. Ding, J. Jiang, A. Shan, Mater. Sci. Eng.: A 509 (1–2) (2009) 76–80.
[26] E.O. Hall, The deformation and ageing of mild steel: III. Discussion of results, Proc. Phys. Soc. Lond. B 64 (9) (1951) 747.
[27] N.J. Petch, The cleavage strength of polycrystals, J. Iron Steel Inst. 174 (1953) 25–28.
[28] E. Anderson, D.W.W. King, J. Spreadborough, Trans. TMS-AIME 242 (1968) 115–119.
[29] W.B. Morrison, Trans. Am. Soc. Met. 59 (1966) 824–846.
[30] R. Armstrong, I. Codd, R.D. Douthwaite, N.J. Petch, Philos. Mag. 7 (1962) 45.
[31] K. Takeda, N. Nakada, T. Tsuchiyama, S. Takaki, ISIJ Int. 48 (2008) 1122–1125.
[32] C.C. Koch, Scr. Mater. 49 (2003) 657.
[33] Y.T. Zhu, B.Q. Han, E.J. Lavernia, M.J. Zehetbauer, Y.T. Zhu (Eds.), Bulk Nanostructured Materials, Wiley-VCH Verlag GmbH & Co, Weinheim, 2009, p. 89.
[34] Y.T. Zhu, T.G. Langdon, JOM 56 (10) (2004) 58.
[35] H. Conrad, Mater. Sci. Eng. A 341 (2003) 216.
[36] K.-T. Park, Y.S. Kim, J.G. Lee, D.H. Shin, Mater. Sci. Eng. A 293 (2000) 165.

[37] Y.M. Wang, E. Ma, Acta Mater. 52 (2004) 1699.
[38] E. Ma, JOM 58 (2006) 49.
[39] F.H. Dalla Torre, A.A. Gazder, E.V. Pereloma, C.H.J. Davies, J. Mater. Sci. 42 (2007) 9097.
[40] R.Z. Valiev, E.V. Kozlov, Y.F. Ivanov, J. Lian, A.A. Nazarov, B. Baudelet, Acta Metall. Mater. 42 (1994) 2467.
[41] R.Z. Valiev, I.V. Alexandrov, Y.T. Zhu, T.C. Lowe, Paradox of strength and ductility in metals processed by severe plastic deformation, J. Mater. Res. 17 (2002) 5–8.
[42] F. Humphreys, M. Hatherly, Recrystallization and Related Annealing Phenomena, Pergamon, 1996.
[43] D. Hughes, N. Hansen, Acta Mater. 48 (2000) 2985.
[44] F.R.N. Nabarro, Z.S. Basinski, D.B. Holt, Adv. Phys. 13 (1964) 193.
[45] Y. Bergström, B. Aronsson, Metall. Trans. 3 (1972) 1951.
[46] L.S. Tóth, A. Molinari, Y. Estrin, J. Eng. Mater. Technol. 124 (2002) 71.
[47] M. Mueller, M. Zehetbauer, A. Borbely, T. Ungar, Z. Met. 86 (1995) 827–831.
[48] M. Zehetbauer, T. Ungár, Priv. Commun. (1997).
[49] Y. Ivanov, A. Panin, A. Son, V. Kopylov, V. Klimenov, Structural analysis of ARMCO iron subjected to equal channel angular extrusion, Russ. Phys. J. 48 (4) (2005) 406–411.
[50] E. Schafler, M. Zehetbauer, A. Borbely, T. Ungar, Mater. Sci. Eng. A Vols. 234–236 (1997) 445–448.
[51] A.S. Argon, P. Haasen, Acta Metall. 41 (1993) 3289.